Mineralogical Magazine (2022), **86**, 134–140
doi:10.1180/mgm.2021.106

CAMBRIDGE UNIVERSITY PRESS

Article

Site splitting at *M*3 in allanite-(Ce)

Can Shen[1], Zhengxiang Shu[1], Xiangping Gu[1], Jeffrey Dick[1], Yuzhou Feng[3], Hui Zheng[3,4] and Anhuai Lu[1,2]*

[1]Key Laboratory of Metallogenic Prediction of Nonferrous Metals and Geological Environment Monitoring, School of Geoscience and Info-Physics, Central South University, Changsha, 410083, China; [2]The Key Laboratory of Orogenic Belts and Crustal Evolution, Beijing Key Laboratory of Mineral Environmental Function, School of Earth and Space Sciences, Peking University, Beijing 100871, China; [3]Guangzhou Institute of Geochemistry, Chinese Academy of Sciences, Guangzhou, 510640, China; and [4]University of Chinese Academy of Sciences, Beijing 100049, China

Abstract

We report the crystal structure of allanite-(Ce), with composition $(Ca_{1.0}REE_{0.9}\square_{0.1})_{\Sigma 2.0}(Al_{1.46}Fe^{3+}_{0.52}Fe^{2+}_{0.76}Mg_{0.12}Ti_{0.15})_{\Sigma 3.01}Si_3O_{12}(OH)$ from the Xinfeng rare earth element (REE)-bearing granite in Guangdong Province, China. It has the unit cell $a = 8.9550(4)$ Å, $b = 5.77875(16)$ Å, $c = 10.2053(4)$ Å, $\beta = 114.929(5)°$ and $Z = 2$ in space group $P2_1/m$ and is characterised by site splitting at *M*3 into *M*3a and *M*3b, at a distance of 0.38(3) Å, which are occupied partially by $Fe_{0.764}Mg_{0.12}$ and $Ti_{0.15}$, respectively. The structure was determined by single-crystal X-ray diffraction and refined with anisotropic full-matrix least-squares refinement on F^2 to $R_1 = 2.82\%$, $wR_2 = 7.77\%$ for 1856 independent reflections (8772 collected reflections). However, *M*3 splitting is not present in either ferriallanite-(Ce) or epidote, in which *M*3 is almost fully occupied either by Fe^{2+} or by Fe^{3+}. Comparisons of bond lengths and volumes in cation polyhedra among allanite-(Ce), ferriallanite-(Ce) and epidote tend to indicate that the essential factor that facilitates site splitting of *M*3 in allanite-(Ce) is heterovalent substitution and occupation of a crystallographic site between $Fe^{2+}(Mg^{2+}/Mn^{2+})$–$Al^{3+}(Ti^{4+})$, a common phenomenon in minerals, such as the plagioclase series. Fine structure analysis of the *M*3 split model revealed that deformation of *A*2 is related closely to distorted *M*3, which is consistent with Fe^{2+} incorporation following REE substitution.

Keywords: allanite-(Ce), structure refinement, site split model, *M*3 octahedron

(Received 22 July 2021; accepted 24 December 2021; Accepted Manuscript published online: 14 January 2022; Associate Editor: Sergey V Krivovichev)

Introduction

Allanite, formula $^{A1}Ca^{A2}REE^{M3}Fe^{M1}Al^{M2}Al(Si_2O_7)(SiO_4)^{O4}O^{O10}(OH)$, a major carrier of rare earth elements (REE), is a group member of the epidote supergroup. The crystal structure consists of two independent edge-sharing octahedral chains along the ***b***-axis, a single *M*2 chain and a 'zig-zag' chain of *M*1 with *M*3 octahedra attached on alternate sites, and Si_2O_7 dimers and SiO_4 islands, with cavities occupied by *A*1 and *A*2 cations (Bonazzi and Menchetti, 1995). Whereas the *A*1 site prefers Ca^{2+}, *A*2 always hosts REE cations (Dollase, 1971; Ercit, 2002). The octahedral positions are distinguished on the basis of distinctive preferential occupancy of Al^{3+}, Fe^{3+}, Fe^{2+}, Mg^{2+} and Mn^{2+} (Armbruster *et al.*, 2006). The species in the group are classified by dominant cations at the *A*2, *M*1, *M*3 and *O*4 key sites. The *M*2 site in allanite is occupied mostly by Al^{3+}, and iron can be incorporated as Fe^{3+}or Fe^{2+}on the *M*1 site, while the *M*3 site is occupied preferably by Fe^{2+}, Mg^{2+}, or Mn^{2+} (Gieré and Sorensen, 2004; Armbruster *et al.*, 2006).

According to the charge-balance coupled substitution: $REE^{3+}(A2) + M^{2+}(M3) = Ca^{2+}(A2) + M^{3+}(M3)$ (Peterson and Macfarlane, 1993), REE substitution happens at the same time as Fe^{2+} incorporation. Crystal structures also show that the *M*3 octahedron shares edges with the REE-bearing *A*2 polyhedron. Because the deformation of the *M*3 octahedron affects the REE-rich *A*2 polyhedron, the presence of divalent cations in *M*3 sites is related to REE content, as well as iron-oxidation and dehydration processes (Reissner *et al.*, 2019, 2020).

During structure determination and refinement of a series of allanite-(Ce) samples, we found that the *M*3 site is split, a phenomenon not reported before for the epidote supergroup. Here, we present the crystal structure of allanite with a site split model at *M*3 and compare it with ferriallanite-(Ce) and epidote, which do not show site splitting. We summarise the differences of their refined structures and discuss the split mechanism and relationship with divalent–trivalent substitution. The crystallographic information files (cif) have been deposited with the Principal Editor of *Mineralogical Magazine* and are available as Supplementary material (see below).

Sample description

The allanite-(Ce) and epidote samples (Fig. 1) were from the central zone of the Xinfeng granite, which is part of the Fogang granitic batholith in Guangdong Province, China. Allanite-(Ce) forms dark brown to black tabular and columnar crystals, up to 2 mm in size, and is associated with epidote, titanite, ilmenite, hastingsite, julgoldite-(Fe^{3+}), biotite, feldspar and quartz. In thin sections, the crystals of allanite-(Ce) are pleochroic with yellow to dark brown colour, and some of them are subject to various degree of metamictisation. Epidote occurs as dark green tabular

*Author for correspondence: Anhuai Lu, Email: ahlu@pku.edu.cn
Cite this article: Shen C., Shu Z., Gu X., Dick J., Feng Y., Zheng H. and Lu A. (2022) Site splitting at *M*3 in allanite-(Ce). *Mineralogical Magazine* **86**, 134–140. https://doi.org/10.1180/mgm.2021.106

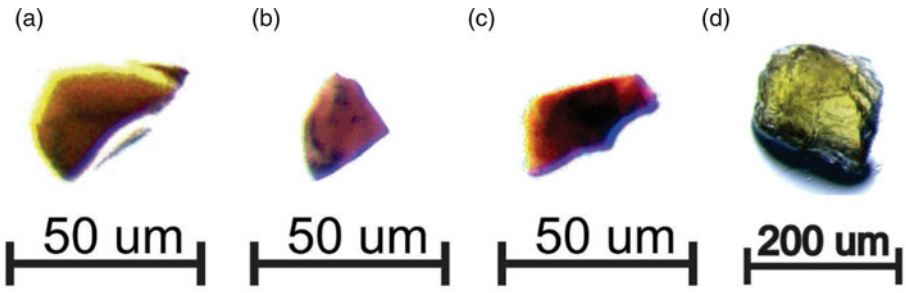

Fig. 1. Single crystals of samples used for structure analysis. Allanite-(Ce) from (a) Xinfeng and (b) Gucheng, Guangdong province, China. (c) Ferriallanite-(Ce) from the Huayangchuan ore deposit in the Qinling Orogen, Central China. (d) Epidote from the Xinfeng granite, Guangdong province, China.

Table 1. Crystal data and final structure refinement for Xinfeng allanite-(Ce), ferriallanite-(Ce) and epidote.

	Allanite-(Ce)	Ferriallanite-(Ce)	Epidote
Crystal data			
Structural formula	$(Ca_{1.00}Ce_{0.46}La_{0.25}Pr_{0.06}Nd_{0.13})_{\Sigma1.9}$ $(Al_{1.51}Fe_{1.26}Ti_{0.15}Mg_{0.12})_{\Sigma3.04}Si_{3.0}O_{12}(OH)$	$(Ca_{0.92}Ce_{0.55}La_{0.28}Pr_{0.04}Nd_{0.06})_{\Sigma1.91}$ $(AlFe_{1.58}Ti_{0.15}Mg_{0.18})_{\Sigma2.99}Si_3O_{12}(OH)$	$Ca_{2.00}(Al_{2.05}Fe_{0.94})_{\Sigma3.00}$ $Si_3O_{12}(OH)$
Crystal size (mm)	0.035×0.030×0.025	0.035×0.03×0.025	0.2×0.2×0.2
Crystal colour	Brown	Brown	Green
Crystal system	Monoclinic	Monoclinic	Monoclinic
Space group	$P2_1/m$	$P2_1/m$	$P2_1/m$
Temperature (K)	293	293	293
a (Å)	8.9550(4)	8.9599(5)	8.9094(3)
b (Å)	5.77875(16)	5.8062(3)	5.65071(15)
c (Å)	10.2053(4)	10.1742(5)	10.1717(4)
β (°)	114.929(5)	114.720(6)	115.404(4)
Volume (Å^3)	478.91(3)	480.79(5)	462.57(3)
Z	2	2	2
ρ_{calc} (g/cm^3), μ (mm^{-1})	4.025, 7.405	4.056, 7.840	3.454, 3.321
F (000)	552.0	558.0	476.0
Data collection			
2θ range (°)	4.402 to 66.792	4.408 to 67.16	4.434 to 67.254
Reflections collected	8772	5810	5217
Reflections independent	1856	1791	1729
R_{int}, R_{sigma}	0.0225, 0.0173	0.0246, 0.0259	0.0183, 0.0189
Data completeness	100%	100%	99.70%
Indices range of *h*	$-13 \le h \le 12$	$-12 \le h \le 12$	$-12 \le h \le 13$
Indices range of *k*	$-8 \le k \le 8$	$-8 \le k \le 7$	$-7 \le k \le 8$
Indices range of *l*	$-15 \le l \le 14$	$-14 \le l \le 15$	$-14 \le l \le 14$
Refinement			
Data/parameters/restraints[1]	1856/131/1	1791/122/1	1729/123/1
Goodness-of fit on F^2	1.063	1.064	1.106
R_1 [$I > 2\sigma(I)$], R_1(all)	0.0282, 0.0307	0.0258, 0.0282	0.0224, 0.0240
wR_2 [$I > 2\sigma(I)$], wR_2(all)	0.0777, 0.0792	0.0734, 0.0750	0.0654, 0.0660
Residual. peak/hole (e^{-3})	1.87/−0.83	1.01/−1.25	0.43/−1.02

[1]DFIX H–O = 0.96 Å

and columnar crystals, up to 3 mm in size. The sample of ferriallanite-(Ce) was from the supergiant carbonatite-hosted Huayangchuan ore deposit in the Qinling Orogen, Central China (Zheng *et al.*, 2020).

Experimental methods

Chemical compositions were analysed with a Shimadzu EPMA-1720 electron probe microanayser at an accelerating voltage of 15 kV, a beam current of 20 nA and beam size of ~2 μm. Pure materials of SiO_2, Al_2O_3, Fe_2O_3, TiO_2, MgO, MnO_2, $CaSiO_3$, and a set of rare earth element phosphates, including LaP_5O_{14}, CeP_5O_{14}, PrP_5O_{14}, NdP_5O_{14} and SmP_5O_{14}, were used for standards. The ZAF3 program provided with the instrument was used for concentration corrections.

Single-crystal diffraction data were collected on a Rigaku XtaLAB Synergy-DW diffractometer with a microfocus sealed Mo anode tube at 50 kV and 1 mA. Depending on the crystal size, the exposure time per frame was set to 2s, 3s or 5s. The experimental data were analysed with Rigaku *CrysAlisPro*, and all reflections were indexed on the basis of a monoclinic unit cell. The systematic absence of reflections suggests the space group $P2_1/m$. The crystal structure was solved with *SHELXT* and refined with *SHELXL* (Sheldrick *et al.*, 1993; Bourhis *et al.*, 2015; Sheldrick, 2015), which are included in the software *Olex2* (Dolomanov *et al.*, 2009). The occupancies for O and Si were fixed at 1 and the occupancies for other cations were refined according to both minimum R_1 value and good agreement with empirical compositions. Anisotropic displacement parameters were refined for all atoms. Data and structure refinement for the crystals are summarised in Table 1.

Results

Chemical compositions

The empirical formula of allanite-(Ce), from the average of 8 analyses, is calculated to be $(Ca_{1.0}REE_{0.9}\square_{0.1})_{\Sigma2.0}(Al_{1.46}Fe^{3+}_{0.52}Fe^{2+}_{0.76}$

https://doi.org/10.1180/mgm.2021.106 Published online by Cambridge University Press

Table 2. Chemical composition of allanite-(Ce), ferriallanite-(Ce) and epidote.

Sample name	Allanite-(Ce)* Aln-XF (n = 8)		Ferriallanite-(Ce) Ferri-aln-HYC (n = 2)		Epidote Ep-XF (n = 10)	
wt.%	Avg.	Std.	Avg.	Std.	Avg.	Std.
MgO	0.78	0.26	1.23	0.04	0.16	0.19
Al_2O_3	12.74	0.79	6.77	0.18	21.99	1.46
SiO_2	30.87	1.12	30.49	0.31	37.79	0.85
CaO	9.56	1.24	8.54	0.05	24.08	0.67
TiO_2	2.03	0.37	2.00	0.13	–	–
La_2O_3	6.98	1.37	7.53	0.76	–	–
Ce_2O_3	13.11	0.91	14.60	0.87	–	–
Pr_2O_3	1.62	0.66	1.06	0.09	–	–
Nd_2O_3	3.65	0.92	1.68	0.02	–	–
FeO*	15.74	1.29	21.55	0.39	14.10	2.14
MnO*	–	–	1.01	0.02	–	–
F	–	–	0.27	0.04	–	–
Total	97.09		96.73		98.13	
Formula	$(Ca_{1-0}REE_{0.9}\square_{0.1})_{\Sigma 2.0}$ $(Al_{1.46}Fe^{3+}_{0.52}Fe^{2+}_{0.76}Mg_{0.12}Ti_{0.15})_{\Sigma 3.01}$ $Si_3O_{12}(OH)$		$(Ca_{0.92}REE_{0.91}\square_{0.17})_{\Sigma 2.0}$ $(Al_{0.80}Fe^{3+}_{1.29}Fe^{2+}_{0.51}Mg_{0.18}Ti_{0.15}Mn_{0.09})_{\Sigma 3.02}$ $Si_3O_{12}[(F_{0.08},(OH)_{0.92}]$		$Ca_{2.0}(Al_{2.05}Fe_{0.94})_{\Sigma 2.99}$ $Si_3O_{12}(OH)$	

*Allanite-(Ce) data is for Xinfeng samples.
**Total Fe calculated as FeO and Mn as MnO; the Fe^{2+}/Fe^{3+} ratio calculated based on charge balance. '–' = not detected.

Table 3. Fractional atomic coordinates of Xinfeng allanite-(Ce) and atom occupancies compared to ferriallanite-(Ce) and epidote.

Sites	Occupancy				x	y	z
	Allanite-(Ce)[1]	Allanite-(Ce)[2]	Ferriallanite-(Ce)[3]	Epidote[1]			
*M*1	$Al_{0.607}Fe_{0.393}(6)$	$Al_{0.688}Fe_{0.312}(7)$	$Ti_{0.15}Fe_{0.76}$	$Al_{0.955}Fe_{0.045}(4)$	0	0	0
*M*2	$Al_{0.900}Fe_{0.100}(6)$	$Al_{0.899}Fe_{0.101}(7)$	$Al_{1.00}$	$Al_{0.973}Fe_{0.027}(4)$	1	0	½
*M*3a	$Fe_{0.764}Mg_{0.12}(5)$	$Fe_{0.739}Mn_{0.04}(5)$	$Fe_{0.82}Mg_{0.18}$	$Fe_{0.87}Al_{0.119}$	0.3032(12)	¼	0.21644(10)
*M*3b	$Ti_{0.15}$	$Ti_{0.11}$	–	–	0.3351(14)	¼	0.1972(11)
*A*1	$Ca_{0.934}Ce_{0.066}(2)$	$Ca_{0.921}Ce_{0.079}(2)$	$Ca_{0.91}Ce_{0.01}$	$Ca_{1.00}$	0.75784(10)	¾	0.15146(9)
*A*2	$REE_{0.837}Ca_{0.06}(6)$	$REE_{0.826}Ca_{0.08}(2)$	$REE_{0.93}Ca_{0.07}$	$Ca_{1.00}$	0.59457(3)	¾	0.42822(3)
Si1	$Si_{1.00}$	$Si_{1.00}$	$Si_{1.00}$	$Si_{1.00}$	0.33856(12)	¾	0.03731(11)
Si2	$Si_{1.00}$	$Si_{1.00}$	$Si_{1.00}$	$Si_{1.00}$	0.68746(12)	¼	0.27832(11)
Si3	$Si_{1.00}$	$Si_{1.00}$	$Si_{1.00}$	$Si_{1.00}$	0.18815(12)	–¼	0.32395(11)
O1	$O_{1.00}$	$O_{1.00}$	$O_{1.00}$	$O_{1.00}$	0.2330(3)	–0.0124(4)	0.0256(2)
O2	$O_{1.00}$	$O_{1.00}$	$O_{1.00}$	$O_{1.00}$	0.3122(3)	–0.0274(4)	0.365(2)
O3	$O_{1.00}$	$O_{1.00}$	$O_{1.00}$	$O_{1.00}$	0.7974(3)	0.0156(4)	0.3366(2)
O4	$O_{1.00}$	$O_{1.00}$	$O_{1.00}$	$O_{1.00}$	0.0588(4)	¼	0.1309(3)
O5	$O_{1.00}$	$O_{1.00}$	$O_{1.00}$	$O_{1.00}$	0.0497(4)	–¼	0.1519(3)
O6	$O_{1.00}$	$O_{1.00}$	$O_{1.00}$	$O_{1.00}$	0.0694(4)	–¼	0.4118(3)
O7	$O_{1.00}$	$O_{1.00}$	$O_{1.00}$	$O_{1.00}$	0.5094(4)	¾	0.1790(3)
O8	$O_{1.00}$	$O_{1.00}$	$O_{1.00}$	$O_{1.00}$	0.5418(4)	¼	0.3302(4)
O9	$O_{1.00}$	$O_{1.00}$	$O_{1.00}$	$O_{1.00}$	0.6114(4)	¼	0.1011(3)
O10	$O_{1.00}$	$O_{1.00}$	$O_{1.00}$	$O_{1.00}$	0.9134(3)	–¼	0.5689(3)
H10	$H_{1.00}$	$H_{1.00}$	$H_{1.00}$	$H_{1.00}$	0.9280(90)	–¼	0.6620(30)

[1]Allanite-(Ce) and epidote from Xinfeng; [2] allanite-(Ce) from Gucheng; [3] ferriallanite-(Ce) from Huayangchuan.

$Mg_{0.12}Ti_{0.15})_{\Sigma 3.01}Si_3O_{12}(OH)$, based on 3(Si) atoms and arbitrary 12(O) and 1(OH) per formula unit (apfu). The REE in allanite-(Ce) are dominated by Ce, La, Nd and Pr, respectively with La = 0.25 apfu, Ce = 0.46 apfu, Pr = 0.06 apfu and Nd = 0.13 apfu. The calculation of charge balance reveals that Fe^{2+} = 0.76 apfu and Fe^{3+} = 0.52 apfu. The empirical formula of epidote is $Ca_{2.0}(Al_{2.05}Fe_{0.94})_{\Sigma 2.99}$ $Si_{3.0}O_{12}(OH)$, from the average of 10 analyses, in which Fe is classified as ferric according to charge balance (Table 2). Ferriallanite-(Ce) from the Huayangchuan deposit (Zheng *et al.*, 2020a) has the empirical formula $(Ca_{0.92}REE_{0.91}\square_{0.17})_{\Sigma 2.0}(Al_{0.8}Fe^{3+}_{1.29}Fe^{2+}_{0.51}Ti_{0.15}Mg_{0.18}Mn_{0.09})_{\Sigma 3.02}$ $Si_{3.0}O_{12}[(F_{0.08},(OH)_{0.92}]$.

Crystal structures

The structures of allanite-(Ce), ferriallanite-(Ce) and epidote are all isostructural with that of the epidote supergroup (Dollase, 1971). Elements with <0.01 apfu were ignored in structure refinement. The fractional atomic coordinates and the occupancies of atoms at the *M*1, *M*2, *M*3, *A*1 and *A*2 sites of allanite-(Ce) are shown in Table 3 for comparison with ferriallanite-(Ce) and epidote. The displacement parameters are shown in Table 4. Table 3 shows that the *M*2 site is dominated by Al with negligible Fe^{3+} in all the three minerals, and *M*1 is dominated by Al with incorporation of minor Fe^{3+} in allanite-(Ce) and epidote, but

https://doi.org/10.1180/mgm.2021.106 Published online by Cambridge University Press

Table 4. Anisotropic and equivalent isotropic displacement parameters for Xinfeng allanite-(Ce) (in Å^2).

Sites	U^{11}	U^{22}	U^{33}	U^{23}	U^{13}	U^{12}	U_{eq}
*M*1	0.0112(4)	0.0103(4)	0.0152(4)	0.0005(3)	0.0047(3)	−0.0005(3)	0.0125(2)
*M*2	0.0102(5)	0.0089(5)	0.0133(5)	−0.0006(3)	0.0038(4)	0.0004(3)	0.0112(3)
*M*3a	0.0092(6)	0.0133(4)	0.0138(4)	0	0.0017(4)	0	0.0124(2)
*M*3b	0.0310(9)	0.0300(5)	0.0400(9)	0	−0.0090(5)	0	0.0032(3)
*A*1	0.0298(4)	0.0142(4)	0.0214(4)	0	0.0161(3)	0	0.0200(2)
*A*2	0.0149(13)	0.02246(15)	0.01457(13)	0	0.00423(10)	0	0.01797(9)
Si1	0.0099(4)	0.0080(4)	0.0104(4)	0	0.0033(3)	0	0.00981(18)
Si2	0.0107(4)	0.0089(4)	0.0116(4)	0	0.0043(3)	0	0.01051(18)
Si3	0.0084(4)	0.0100(4)	0.0097(4)	0	0.0043(3)	0	0.00922(18)
O1	0.0157(9)	0.0113(9)	0.0241(10)	0.0021(7)	0.0094(8)	0.0020(7)	0.0167(4)
O2	0.0167(9)	0.0160(9)	0.0158(9)	−0.0014(7)	0.0068 (7)	−0.0053(7)	0.0162(4)
O3	0.0141(8)	0.0113(8)	0.0180(9)	−0.0017(7)	−0.0003(7)	0.0014(7)	0.0169(4)
O4	0.0115(12)	0.0161(13)	0.0165(13)	0	0.0037(10)	0	0.0154(5)
O5	0.0128(12)	0.0166(13)	0.0134(12)	0	0.0041(10)	0	0.0148(5)
O6	0.0142(11)	0.0117(12)	0.0153(12)	0	0.0092(10)	0	0.0128(5)
O7	0.0157(13)	0.0200(14)	0.0131(12)	0	0.0012(10)	0	0.0180(6)
O8	0.0164(14)	0.0410(2)	0.0230(16)	0	0.0112(12)	0	0.0260(7)
O9	0.0205(14)	0.0311(17)	0.0129(13)	0	0.0078(11)	0	0.0212(6)
O10	0.0125(12)	0.0126(12)	0.0162(11)	0	0.0079(10)	0	0.0131(5)
H10							0.0400(2)

Fe^{3+} dominates *M*1 in ferriallanite-(Ce). The *M*3 site is dominated by iron in all three minerals. It is remarkable that the *M*3 site is split in allanite-(Ce) but not in ferriallanite-(Ce) and epidote. To confirm this, two more crystals of allanite-(Ce) from Xinfeng and Gucheng, in the Guangdong province, China were also checked by single-crystal diffraction, and all have split *M*3 sites at a distance of 0.38(3) Å, which are hereafter designated as *M*3a and *M*3b. In allanite-(Ce) from Xinfeng, *M*3a is partially occupied by $Fe_{0.76}Mg_{0.12}$ and *M*3b and partially occupied by $Ti_{0.15}$. In allanite-(Ce) from Gucheng, *M*3a is partially occupied by $Fe_{0.74}Mn_{0.04}$ and *M*3b is partially occupied by $Ti_{0.11}$ (Table 3). The site splitting of *M*3 in allanite-(Ce) is required for the structure to be acceptable as the maximum peak residual is 3.60 e^{-3}. In addition R_1 is larger (3.10%) before the site splitting (Table 6).

The 7-coordinated *A*1 is almost fully occupied by Ca in the three minerals, whereas the 11-coordinated *A*2 is dominated by rare earth elements in allanite-(Ce) and ferriallanite-(Ce) but is dominated by Ca in epidote. The occupancies of Ce, La, Nd and Pr for the *A*2 site were fixed based on chemical compositions. The tetrahedral sites *Si*1, *Si*2 and *Si*3 are fully occupied by Si (Fig. 2a, 2b). In structure refinement, the bond lengths (*r*) connected to O10 are 1.91 Å and 2.60 Å for <*O*10–*M*2>×2 and <*O*10–*A*2>, respectively. The bond valance, s, estimated by using the bond-valance equation $s = \exp[(r_0 - r)]/B$ (Brown and Altermatt, 1985; Brese and O'Keeffe, 1991), sums to −1.22 for O10. This suggests that the hydrogen position is located on it, which is consistent with most reported allanite structures.

Bond distances, polyhedral volumes, site distortion index, and bond angle variance of allanite-(Ce), ferriallanite-(Ce) and epidote are summarised in Table 5 (calculated according to quadratic elongation (Robinson *et al.*, 1971) using *VESTA* (Momma and Izumi, 2011)). These results show that *M*1 is linked to O1, O4 and O5 to form a nearly normal octahedron in epidote, but the substitution by Fe^{3+} in allanite-(Ce) and ferriallanite-(Ce) leads to slight expansion and distortion of the volume of *M*1. The *M*2 cation is linked to O3, O6 and the hydroxyl O10 with little change in the *M*2–O bond length, leading to the smallest and most regular octahedron. $M3a_{Fe/Mg}$ and $M3b_{Ti}$ cations, which are split from *M*3, are connected to six oxygens to form the most distorted octahedron *M*3b ($\sigma^2_{allanite\text{-}M3b} > \sigma^2_{epidote\text{-}M3} > \sigma^2_{ferriallanite\text{-}M3} > \sigma^2_{allanite\text{-}M3a}$). The incorporation of a higher amount of Fe^{2+} causes the greater volume ($V_{ferriallanite\text{-}M3} > V_{allanite\text{-}M3} > V_{epidote\text{-}M3}$) and higher average bond length.

The mean distance of *A*1–O is similar among these three samples, while further variation occurs with the incorporation of REE cations in the *A*2 polyhedron with face-shared geometry (O7–O3–O3). O7 and O3 move away from the *A*1 site as the *A*1–O1 bond shortens. The longer bonds of *A*2 cause the polyhedron volume to be twice that of *A*1. The *A*2–O2 bonds shorten to balance the lowered bond strength of *A*2–O3, *A*2–O7 and *A*2–O10, which accompanies the unequal substitution of REE cations by Ca^{2+} (Table 5).

Tetrahedra are the most stable unit in the allanite structure. The distance between Si and O in every tetrahedron can be considered as a constant (Table 5), and there is no substitution of Si by other cations. The Si3 island near the *b* axis shares O2–O2' edges with the *A*2 octahedron, and thus compresses the O2–Si3–O2' angle to 103.78(17)° and causes a larger variation of bond angles in allanite-(Ce) ($\omega_{Si3} = 27.1 > \omega_{Si1} = 9.9 > \omega_{Si2} = 2.5$). The Si1 and Si2 islands are linked to form an Si_2O_7 dimer in which O9 connects Si1 and Si2 with an Si1–O9–Si2 angle of 143.7(2)°. With the incorporation of REE, the Si1–O9–Si2 angle reduces from 153.39(14)° [epidote] to 143.6(2)° [ferriallanite-(Ce)) and 143.7(2)° (allanite-(Ce)].

Discussion

Refined structure data for the allanite subgroup are listed in Table 6. Much previous work has ignored the residual of the Q peaks, but here we use it to emphasise the site splitting model of Fe^{2+}/Mg^{2+} or Fe^{2+}/Mn^{2+} – Ti^{4+} in allanite when refining the structure. A better *R* factor and more reasonable Q peak residuals were obtained with the site split model of allanite, whereas the one atom model was feasible for ferriallanite-(Ce) and epidote. This shows that Fe^{2+} substituted for Fe^{3+} or Fe^{3+} substituted for Al^{3+} in *M*3 cannot cause the site split. Thus, we conclude that heterovalent substitution leads to the crystal site splitting phenomenon. Similar examples were reported in intermediate plagioclases where the Na^{+}/Ca^{2+} substitution series occurs as

https://doi.org/10.1180/mgm.2021.106 Published online by Cambridge University Press

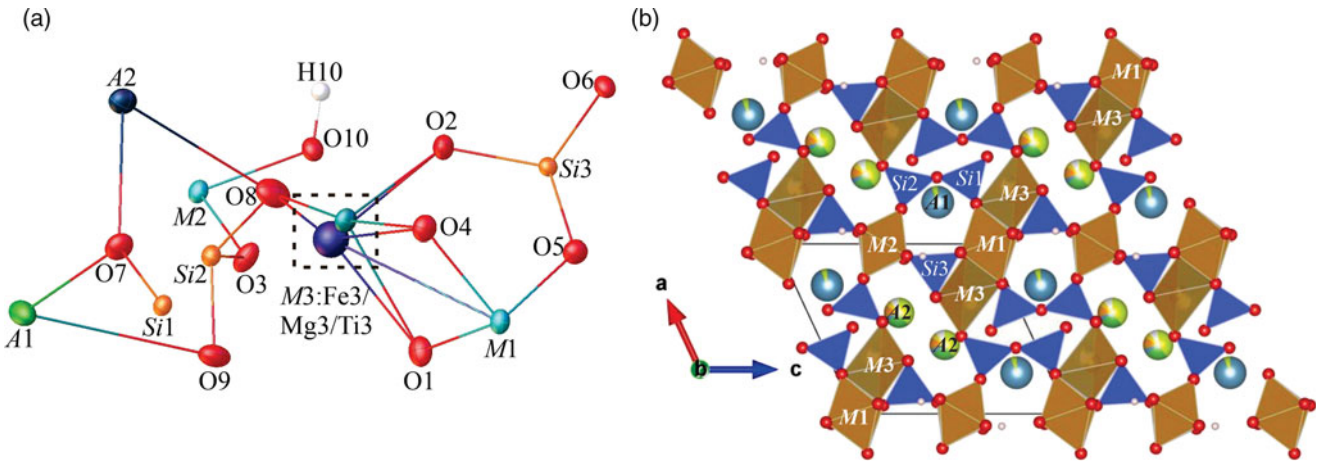

Fig. 2. (a) Molecular structure of allanite-(Ce) showing the split sites; (b) refined polyhedral style structure of allanite-(Ce) projected down the ***b*** axis.

Table 5. Selected bond distance (Å), polyhedral volumes (V = Å^3), distortion index (σ^2) and bond angle variance* (ω = degree^2) for *A*, *M*, *Si* sites for Xinfeng allanite-(Ce).

Bonds	Allanite-(Ce) Distance	Ferriallanite-(Ce) Distance	Epidote Distance	Bonds	Allanite-(Ce) Distance	Ferriallanite-(Ce) Distance	Epidote Distance
*A*1–O3(×2)	2.343(2)	2.342(2)	2.327(2)	*M*1–O4(×2)	1.886(2)	1.922(2)	1.851(2)
*A*1–O1(×2)	2.387(2)	2.376(2)	2.457(2)	*M*1–O1(×2)	1.992(2)	2.038(2)	1.944(2)
*A*1–O7	2.357(3)	2.354(3)	2.303(2)	*M*1–O5(×2)	2.026(2)	2.051(2)	1.966(2)
*A*1–O5	2.612(3)	2.592(3)	2.565(2)	Mean	1.9680	2.0035	1.9202
*A*1–O6	2.932(3)	2.920(3)	2.884(2)	V^{VI} (*M*1)	10.0946	10.6747	9.3627
Mean	2.4798	2.4718	2.4745	σ^2(*M*1)	0.02788	0.02717	0.02405
V^{VII} (*A*1)	19.4996	19.5707	18.9433				
σ^2(*A*1)	0.06716	0.06566	0.05787	*M*2–O3(×2)	1.879(2)	1.887(2)	1.860(2)
				*M*2–O10(×2)	1.908(2)	1.921(3)	1.876(2)
*A*2–O7	2.328(3)	2.337(3)	2.247(2)	*M*2–O6(×2)	1.938(2)	1.941(3)	1.932(2)
*A*2–O2 (×2)	2.505(2)	2.496(2)	2.531(2)	Mean	1.9084	1.9170	1.8890
*A*2–O10	2.589(3)	2.601(3)	2.528(2)	V^{VI} (*M*2)	9.1786	9.3040	8.9288
*A*2–O2 (×2)	2.673(2)	2.646(2)	2.779 (2)	σ^2(*M*2)	0.0103	0.01076	0.01515
*A*2–O3 (×2)	2.810(3)	2.824(2)	2.681 (2)				
*A*2–O8(×3)	3.029(2)	3.032(9)	3.022(7)	*M*3a–O8	1.955(4)	1.957(3)	1.864(2)
Mean	2.7387	2.7336	2.6800	*M*3a–O4	1.986(3)	2.001(3)	1.949(2)
V^{X} (*A*2)	44.8312	44.6169	38.4532	*M*3a–O2(×2)	2.184(2)	2.219(2)	1.997(2)
σ^2(*A*2)	0.07874	0.07836	0.06592	*M*3a–O1(×2)	2.336(2)	2.323(2)	2.241(2)
				Mean	2.1634	2.1738	2.0481
*Si*1–O7	1.602(3)	1.592(3)	1.570(2)	V^{VI} (*M*3)	12.7659	12.9632	11.0482
*Si*1–O1(×2)	1.647(2)	1.643(2)	1.653(2)	σ^2(*M*3)	0.05956	0.05963	0.06268
*Si*1–O9	1.652(3)	1.643(3)	1.639(2)				
Mean	1.6347	1.6301	1.6287	*M*3b–O1(×2)	2.203(8)		
V^{IV} (*Si*1)	2.2330	2.2137	2.2077	*M*3b–O2(×2)	2.417(8)		
σ^2(*Si*1)	0.0100	0.0117	0.0181	*M*3b–O8	1.775(2)		
ω	9.9127	10.3905	9.8492	*M*3b–O4	2.274(2)		
				Mean	2.2146		
*Si*2–O3(×2)	1.632(2)	1.635(2)	1.619(2)	V^{VI} (*M*3)	12.7659		
*Si*2–O8	1.602(3)	1.609(3)	1.597(2)	σ^2(*M*3)	0.06971		
*Si*2–O9	1.642(3)	1.642(3)	1.635(2)				
Mean	1.6274	1.6303	1.6172	*Si*3–O2(×2)	1.631(2)	1.631(2)	1.630(2)
V^{IV} (*Si*2)	2.2099	2.2212	2.1683	*Si*3–O6	1.647(3)	1.648(3)	1.643(3)
σ^2(*Si*2)	0.008	0.0066	0.0064	*Si*3–O5	1.663(3)	1.662(3)	1.670(2)
ω	2.5128	3.1324	3.3415	Mean	1.649	1.6428	1.6431
				V^{IV} (*Si*3)	2.276	2.2453	2.261
				σ^2(*Si*3)	0.0082	0.0075	0.0083
				ω	27.0771	36.1596	18.3929

*Bond distances, polyhedral volumes, distortion index and bond angle variance are calculated according to Robinson *et al.* (1971) using VESTA (Momma and Izumi, 2011).

continuous solid solutions (Yamamoto *et al.*, 1984; Steurer and Jagodzinski, 1988).

The size of the *M*3 octahedron follows the order ferriallanite-(Ce) > allanite-(Ce) > epidote, suggesting that Fe^{2+} content dominates the expansion of *M*3. The volume of allanite octahedra decreases in the sequence $M3bO_6 = M3aO_6 > M1O_6 > M2O_6$, which implies that site splitting also contributes to the expansion of *M*3. Moreover, the large deformation index of *M*3 in these three minerals, especially in

https://doi.org/10.1180/mgm.2021.106 Published online by Cambridge University Press

Table 6. Cation site occupancies and refined parameters of Xinfeng allanite-(Ce) with site split model compared with epidote, ferriallanite and other 'allanites'.

Species	Site occupancy						Refinement	
	*M*1	*M*2	*M*3a	*M*3b	*A*1	*A*2	R_1 (%)	$\Delta\rho_{max}$, $\Delta\rho_{min}$ (e^{-3})
Allanite-(Ce) Split model*	$Fe^{3+}_{0.39}Al^{3+}_{0.61}$	$Fe^{3+}_{0.100}Al^{3+}_{0.900}$	$Fe^{2+}_{0.76}Mg^{2+}_{0.12}$	$Ti^{4+}_{0.15}$	$Ca^{2+}_{0.93}Ce^{3+}_{0.07}$	$Ce^{3+}_{0.4}La^{3+}_{0.25}Pr^{3+}_{0.06}Nd^{3+}_{0.13}Ca^{2+}_{0.06}$	2.82	1.87, −0.80
Allanite-(Ce) 1-atom model*	$Fe^{3+}_{0.39}Al^{3+}_{0.61}$	$Fe^{3+}_{0.100}Al^{3+}_{0.900}$	$Fe^{2+}_{0.74}Mg^{2+}_{0.12}Ti^{4+}_{0.15}$		$Ca^{2+}_{0.93}Ce^{3+}_{0.07}$	$Ce^{3+}_{0.4}La^{3+}_{0.25}Pr^{3+}_{0.06}Nd^{3+}_{0.13}Ca^{2+}_{0.06}$	3.10	3.60, −1.00
Epidote*	$Fe^{3+}_{0.045}Al^{3+}_{0.955}$	$Fe^{3+}_{0.027}Al^{3+}_{0.973}$	$Fe^{3+}_{0.87}Al^{3+}_{0.12}$		$Ca^{2+}_{1.00}$	$Ca^{2+}_{1.00}$	2.24	0.43, −1.02
Allanite-(Ce)[a]	$Fe^{3+}_{0.34}Al^{3+}_{0.66}$	$Al^{3+}_{1.00}$	$Fe^{2+}_{0.83}Al^{3+}_{0.17}$		$Ca^{2+}_{1.00}$	$Ce^{3+}_{0.74}Ca^{2+}_{0.26}$	6.20	–
Allanite-(La)[b]	$Fe^{3+}_{0.34}Al^{3+}_{0.66}$	$Al^{3+}_{1.00}$	$Fe^{2+}_{0.88}Mg^{2+}_{0.12}$		$Ca^{2+}_{1.00}$	$La^{3+}_{0.67}Ca^{2+}_{0.31}$	3.28	3.08, −1.70
Allanite-(Ce)[c]	$Fe^{3+}_{0.18}Al^{3+}_{0.76}Ti^{4+}_{0.06}$	$Al^{3+}_{1.00}$	$Fe^{2+}_{0.73}Fe^{3+}_{0.17}Mg^{3+}_{0.10}$		$Ca^{2+}_{0.81}Mn^{2+}_{0.06}Fe^{2+}_{0.13}$	$Ce^{3+}_{0.34}La^{3+}_{0.22}Pr^{3+}_{0.05}Nd^{3+}_{0.13}Ca^{2+}_{0.22}Sm^{3+}_{0.02}Th^{3+}_{0.02}$	4.25	4.26, −2.24
Ferriallanite-(Ce)*	$Fe^{3+}_{0.76}Ti^{4+}_{0.15}$	$Al^{3+}_{1.00}$	$Fe^{2+}_{0.82}Mg^{2+}_{0.18}$		$Ca^{2+}_{0.91}Ce^{3+}_{0.01}$	$Ce^{3+}_{0.54}La^{3+}_{0.28}Pr^{3+}_{0.04}Nd^{3+}_{0.06}Ca^{2+}_{0.01}$	2.50	1.01, −1.25
Ferriallanite-(Ce)[d]	$Fe^{3+}_{0.8}Al^{3+}_{0.06}Ti^{4+}_{0.14}$	$Fe^{3+}_{0.56}Al^{3+}_{0.44}$	$Fe^{2+}_{0.93}Mn^{3+}_{0.07}$		$Ca^{2+}_{0.97}Ce^{3+}_{0.03}$	$Ce^{3+}_{0.89}Ca^{2+}_{0.11}$	2.60	–
Ferriallanite-(Ce)[e]	$Fe^{3+}_{0.72}Al^{3+}_{0.23}Ti^{4+}_{0.05}$	$Fe^{3+}_{0.82}Al^{3+}_{0.18}$	$Fe^{2+}_{0.97}Al^{3+}_{0.03}$		$Ca^{2+}_{1.00}$	$Ce^{3+}_{0.48}La^{3+}_{0.33}Pr^{3+}_{0.07}Nd^{3+}_{0.12}$	1.57	1.00, −0.68

*This work; [a]Dollase (1971); [b]Orlandi and Pasero (2006); [c]Hoshino *et al.* (2005); [d]Kartashov (2002); [e]Nagashima *et al.* (2011).

site *M*3b, implies that the distortion of the crystal cell is not only caused by different ionic radii but also by the possible crystal site splitting.

Allanite is a common accessory mineral in granite (Hanson *et al.*, 2012) and volcanic (Chesner and Ettlinger, 1989; Hoshino *et al.*, 2010) and metamorphic rocks (Wing *et al.*, 2003). As a major carrier of rare earth elements (REE), the coupled substitution: $Ca^{2+}(A2) + Fe^{3+}/Al^{3+}(M3) = REE^{3+}(A2) + Fe^{2+}/Mg^{2+}/Mn^{2+}(M3)$ between *M*3 and *A*2 sites maintains charge balance in allanite-(Ce). This substitution mechanism is responsible for REE incorporation in the allanites studied.

Conclusions

Based on crystal chemistry and structure refinement of allanite-(Ce), ferriallanite-(Ce) and epidote under the constraint of their compositions, we conclude that the *M*3 site splitting model helps to obtain a better structure that accommodates heterovalent substitution in allanite subgroup minerals. A higher distortion index implies that both different ionic radii and the site split contribute to crystal lattice distortion.

Acknowledgements. This research was funded by the National Natural Science Foundation of China (grant No.42072054) and Central South University (grant No. 2018zzts034).

Supplementary material. To view supplementary material for this article, please visit https://doi.org/10.1180/mgm.2021.106

References

Armbruster T., Bonazzi P., Akasaka M., Bermanec V., Chopin C., Gieré R., Heuss-Assbichler S., Liebscher A., Menchetti S., Pan Y. and Pasero M. (2006) Recommended nomenclature of epidote-group minerals. *European Journal of Mineralogy*, **18**, 551–567.

Bonazzi P. and Menchetti S. (1995) Monoclinic members of the epidote group: effects of the Al ⇌ Fe^{3+} ⇌ Fe^{2+} substitution and of the entry of REE^{3+}. *Mineralogy and Petrology*, **53**, 133–153.

Bourhis L.J., Dolomanov O. V., Gildea R.J., Howard J.A.K. and Puschmann H. (2015) The anatomy of a comprehensive constrained, restrained refinement program for the modern computing environment – Olex2 dissected. *Acta Crystallographica*, **A71**, 59–75.

Brese N.E. and O'Keeffe M. (1991) Bond-valence parameters for solids. *Acta Crystallographica*, **B47**, 192–197.

Brown I.D. and Altermatt D. (1985) Bond-valence parameters obtained from a systematic analysis of the Inorganic Crystal Structure Database. *Acta Crystallographica*, **B41**, 244–247.

Chesner C.A. and Ettlinger A.D. (1989) Composition of volcanic allanite from the Toba Tuffs, Sumatra, Indonesia. *American Mineralogist*, **74**, 750–758.

Dollase W.A. (1971) Refinement of the crystal structures of epidote, allanite, and hancockite. *American Mineralogist*, **56**, 447–464.

Dolomanov O. V., Bourhis L.J., Gildea R.J., Howard J.A.K. and Puschmann H. (2009) OLEX2: A complete structure solution, refinement and analysis program. *Journal of Applied Crystallography*, **42**, 339–341.

Ercit T.S. (2002) The mess that is "Allanite." *Canadian Mineralogist*, **40**, 1411–1419.

Gieré R. and Sorensen S.S. (2004) Allanite and other: REE-rich epidote-group minerals. Pp. 431–493 in: *Epidotes* (A. Liebscher and G. Franz, editors) *Reviews in Mineralogy and Geochemistry*, **56**. Mineralogical Society of America and the Geochemical Society, Washington DC.

Hanson S.L., Falster A.U., Simmons W.B. and Brown T.A. (2012) Allanite-(Nd) from the Kingman feldspar mine, Mojave pegmatite district, Northwestern Arizona, USA. *The Canadian Mineralogist*, **50**, 815–824.

Hoshino M., Kimata M., Nishida N., Kyono A., Shimizu M. and Takizawa S. (2005) The chemistry of allanite from the Daibosatsu Pass, Yamanashi, Japan. *Mineralogical Magazine*, **69**, 403–423.

Hoshino M., Kimata M., Chesner C.A., Nishida N., Shimizu M. and Akasaka T. (2010) Crystal chemistry of volcanic allanites indicative of naturally induced oxidation-dehydrogenation. *Mineralogy and Petrology*, **99**, 133–141.

Kartashov P.A.M. (2002) Ferriallanite-(Ce), $CaCeFe^{3+}AlFe^{2+}(SiO_4)(Si_2O_7)O(OH)$, a new member of the epidote group: Description, X-ray and Mössbauer Study. *The Canadian Mineralogist*, **40**, 1641–1648.

Momma K. and Izumi F. (2011) VESTA 3 for three-dimensional visualization of crystal, volumetric and morphology data. *Journal of Applied Crystallography*, **44**, 1272–1276.

Nagashima M., Imaoka T. and Nakashima K. (2011) Crystal chemistry of Ti-rich ferriallanite-(Ce) from Cape Ashizuri, Shikoku Island, Japan. *American Mineralogist*, **96**, 1870–1877.

Orlandi P. and Pasero M. (2006) Allanite-(La) from Buca Della Vena mine, Apuan Alps, Italy, an epidote-group mineral. *The Canadian Mineralogist*, **44**, 63–68.

Peterson R.C. and Macfarlane D.B. (1993) The rare-earth-element chemistry of allanite from the Grenville Province. *The Canadian Mineralogist*, **31**, 159–166.

Reissner C.E., Bismayer U., Kern D., Reissner M., Park S., Zhang J., Ewing R.C., Shelyug A., Navrotsky A., Paulmann C., Škoda R., Groat L.A., Pöllmann H. and Beirau T. (2019) Mechanical and structural properties of radiation-damaged allanite-(Ce) and the effects of thermal annealing. *Physics and Chemistry of Minerals*, **46**, 921–933.

Reissner C.E., Reissner M., Kern D., Pöllmann H. and Beirau T. (2020) Iron sites in radiation-damaged allanite-(Ce): the effects of thermally induced oxidation and structural reorganization. *Hyperfine Interactions*, **241**, 1–6.

Robinson K., Gibbs G.V. and Ribbe P.H. (1971) Quadratic elongation: a quantitative measure of distortion in coordination polyhedra. *Science*, **172**, 567–570.

Sheldrick G.M. (2015) SHELXT - Integrated space-group and crystal-structure determination. *Acta Crystallographica*, **A71**, 3–8.

Sheldrick G.M., Dauter Z., Wilson K.S., Hope H. and Sieker L.C. (1993) The application of direct methods and Patterson interpretation to high-resolution native protein data. *Acta Crystallographica*, **D49**, 18–23.

Steurer W. and Jagodzinski H. (1988) The incommensurately modulated structure of an andesine (An_{38}). *Acta Crystallographica*, **B44**, 344–351.

Wing B.A., Ferry J.M. and Harrison T.M. (2003) Prograde destruction and formation of monazite and allanite during contact and regional metamorphism of pelites: Petrology and geochronology. *Contributions to Mineralogy and Petrology*, **145**, 228–250.

Yamamoto A., Nakazawa H., Kitamura M. and Morimoto N. (1984) The modulated structure of intermediate plagioclase feldspar $Ca_xNa_{1-x}Al_{1+x}Si_{3-x}O_8$. *Acta Crystallographica*, **B40**, 228–237.

Zheng H., Chen H., Wu C., Jiang H., Gao C., Kang Q., Yang C., Wang D. and Lai C. Kit. (2020) Genesis of the supergiant Huayangchuan carbonatite-hosted uranium-polymetallic deposit in the Qinling Orogen, Central China. *Gondwana Research*, **86**, 250–265.

https://doi.org/10.1180/mgm.2021.106 Published online by Cambridge University Press